Supporting Information

In situ ligand exchange-mediated 0D/1D transformation of a polyoxovanadate

M. Wendt, P. Polzin, J. van Leusen, C. Näther, P. Kögerler, W. Bensch

Figure S1 (SEM micrographs) of the educt[1] $\{Ni(en)_3\}_3[V_{15}Sb_6O_{42}(H_2O)] \cdot \approx 15H_2O$ (**I**) and of the resulting new product $\{Ni(phen)_3\}_2[\{Ni(en)_2\}V_{15}Sb_6O_{42}(H_2O)] \cdot 19H_2O$ (**II**) after reaction with $[Ni(phen)_3](ClO_4)_2 \cdot 0.5H_2O$. EDX data are listed in Table S1.

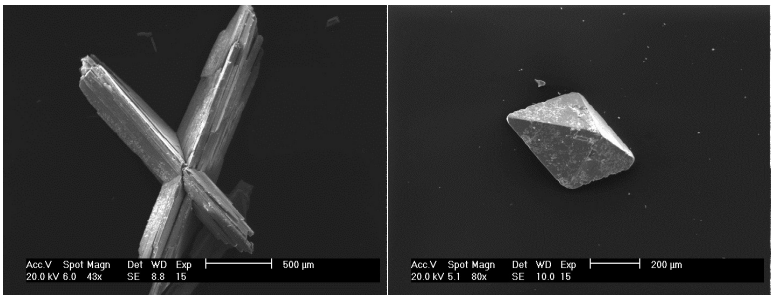

Figure S1. SEM pictures of the precursor $\{Ni(en)_3\}_3[V_{15}Sb_6O_{42}(H_2O)] \cdot \approx 15H_2O$ (left) (**I**) and of $\{Ni(phen)_3\}_2[\{Ni(en)_2\}V_{15}Sb_6O_{42}(H_2O)] \cdot 19H_2O$ (right) (**II**).

Table S1. EDX data compared to the calculated values of $\{Ni(phen)_3\}_2[\{Ni(en)_2\}V_{15}Sb_6O_{42}(H_2O)] \cdot 19H_2O$.

	V [%]	**Sb [%]**	**Ni [%]**
Measured	45.08	44.46	10.46
calculated	45.74	43.72	10.54

The TG curve of **II** displays a first step with a mass loss of Δm = 8 % up to 200 °C indicating the loss of ca. 19 H_2O molecules ($\Delta m_{calculated}$ = 8.7%). The losses of the ethylenediamine and phenanthroline ligands could be occur as next steps, but the POV cluster shell decomposes above 600 °C[1] and there are no clear steps until this temperature, which can be surely assigned to those mass losses (Figure S2). The residual powder was investigated by CHN analysis and revealed that the sample does not contain C, H or N. XRPD analysis showed reflections of VO, V_2O_3 Sb_2O_3 and NiSb.

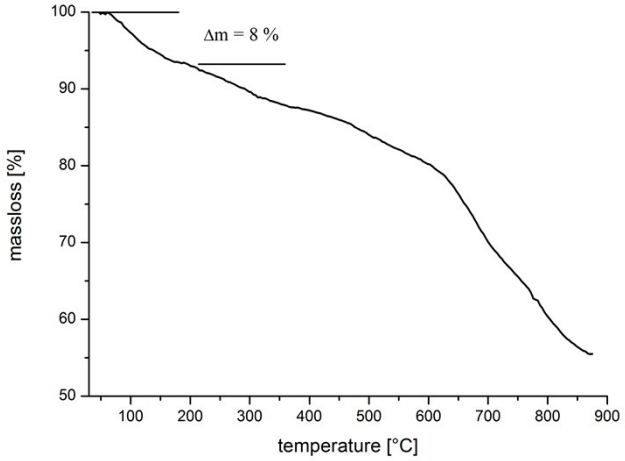

Figure S2. The TG curve of **II**.

Table S2 and Figure S3 display the characteristic vibrations in the IR spectrum of **II** resulting in a characteristic V-O vibration, O-H vibrations of the water molecules and the organic vibrations corresponding to the amine ligands of the complexes.

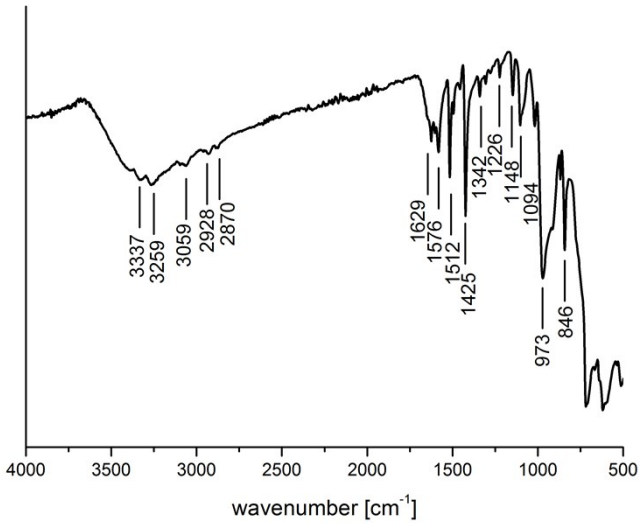

Figure S3. IR spectrum of **II** reveals all significant vibrations of V^{IV}=O and of the aliphatic and aromatic amine ligands.

Table S2. Assignment of the IR bands of compound **II**.

wavenumber [cm^{-1}]	assignment
3600-2700	crystal water
3259	crystal water, NH_2-stretch
3059	crystal water, NH_2-stretch
2928	CH_2 aliphatic
2870	CH_2 aliphatic
1629	C=C aromatic
1576	NH_2 deformation
1512	NH_2 deformation
1425	CH_2 aliphatic
1342	OH deformation
973	V^{IV}=O stretch
846	M-O-M stretch

The XRPD pattern demonstrates phase purity of the sample comparing a measured pattern of **II** with the calculated one obtained from the single crystal structure refinement (Figure S4).

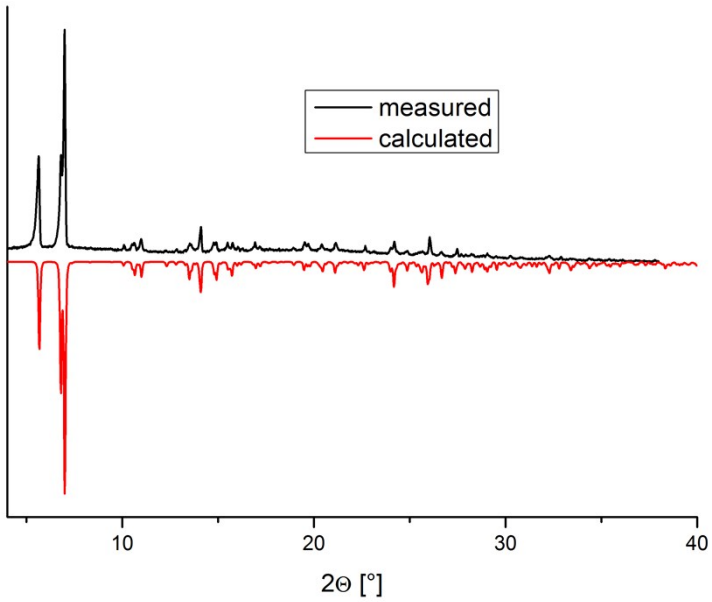

Figure S4: Calculated (red) and measured (black) XRPD pattern of **II**.

Further experiments to validate the ligand exchange were performed using pure phenanthroline (Fig. S5 a)), $[Eu(phen)_2(NO_3)_3]$ (Fig. S5 b)) or $[Cr(phen)_2Cl_2]Cl$ (Fig. 5 c)). Using an excess of $[Ni(phen)_3](ClO_4)_2 \cdot 0.5H_2O$ afforded needles of the complex, which could be separated mechanically. All powder patterns display a good agreement with the calculated pattern obtained from the single crystal structure refinement.

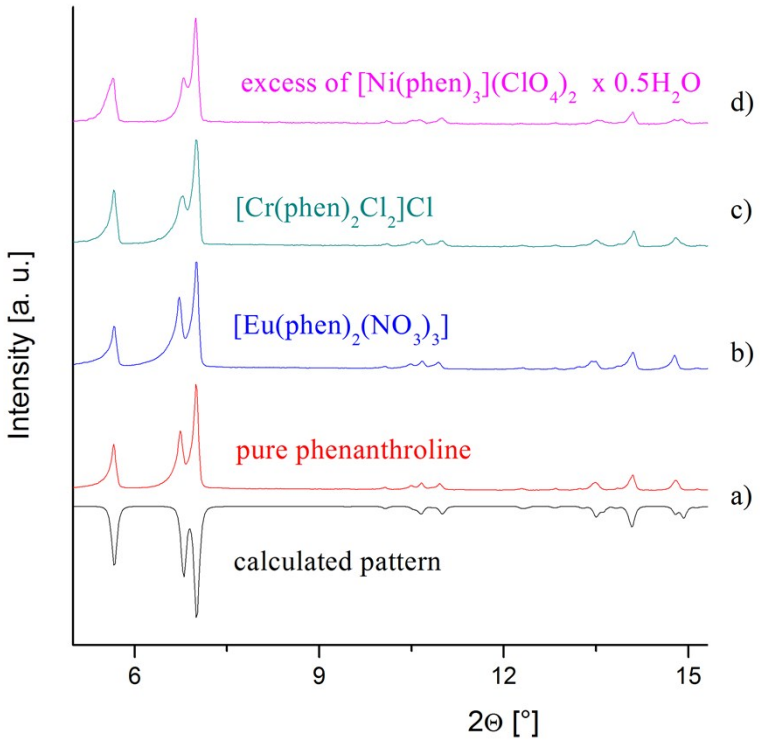

Figure S5: Powder patterns of reaction products after reacting compound **I** with a) phenanthroline, b) $[Eu(phen)_2(NO_3)_3]$, c) $[Cr(phen)_2Cl_2]Cl$ complex and d) an excess of $[Ni(phen)_3](ClO_4)_2 \cdot 0.5H_2O$. Black trace: calculated pattern of compound **II**.

Table S3. Selected crystal data and details of the structure refinement.

	II
Formula	$C_{76}H_{104}Ni_3N_{16}V_{15}Sb_6O_{62}$
MW / g·mol^{-1}	3904.48
crystal system	monoclinic
space group	*C*2/*c*
a /Å	21.2523(12)
b / Å	31.159(2)
c / Å	18.7101(11)
α	90°
β	92.117(7)°
γ	90°
V / Å^3	12381.2(14)
T / K	200
Z	4
D_{calc} / Mg·m^3	2.095
μ / mm^{-1}	2.898
θ_{max}	27.004°
measured refl.	65692
unique refl.	13450
R_{int}	0.0454
$R_1[F_0>4\sigma(F_0)]$	0.0326
wR_2 (all refl.)	0.0925
GOF	1.045

The values for the bond lengths, angles and calculated BVS[2] for the oxidation states are all in a typical range reported for the $\{V_{15}Sb_6O_{42}\}$ cluster shell.[3,4,5,6,7,8,9] The BVS values range from 3.924 (V4) to 3.981 (V6) (average: 3.952) and 3.317 (Sb1) to 3.535 (Sb3) (average: 3.447).

The bond lengths for V-O_a (terminal V=O bond) are between 1.597 and 1.643 Å (average: 1.619 Å); Sb-O_b bond lengths (Sb-O-Sb bond) are 1.930 – 1.944 Å (average: 1.938 Å); V-O_c bonds (V_2-O-Sb bonds) range from 1.931 to 2.022 Å (average: 1.979 Å) and the V-O_d bonds (V_2-O-V bond) are between 1.902 and 1.963 Å (average: 1.933 Å) (Table S4). Table S5 represents Ni-O and Ni-N bond lengths and angles. The interatomic distances and O-H···O/N angles are summarized in Table S6.

Table S4. Bond lengths of the four different oxygen atom types in Å of **II**.

Type	Atom	V	V	V	Sb	Sb
Oa	O11	1.616(2)				
Oa	O13	1.597(4)				
Oa	O16	1.643(2)				
Oa	O17	1.634(2)				
Oa	O19	1.619(2)				
Oa	O20	1.619(2)				
Oa	O21	1.610(2)				
Oa	O22	1.618(2)				
Ob	O3				1.935(2)	1.930(3)
Ob	O7				1.944(1)	1.944(2)
Oc	O1	1.972(2)	1.985(2)		1.967(2)	
Oc	O2	1.995(2)	1.998(2)		1.979(2)	
Oc	O4	1.972(2)	1.979(2)		1.944(2)	
Oc	O5	2.011(2)	1.987(2)		1.950(2)	
Oc	O6	2.000(2)	1.979(2)		1.931(2)	
Oc	O8	2.022(2)	2.008(2)		1.934(2)	
Od	O9	1.936(2)	1.934(2)	1.948(2)		
Od	O10	1.928(2)	1.948(2)	1.949(2)		
Od	O12	1.963(2)	1.952(2)	1.959(2)		
Od	O14	1.919(2)	1.929(2)	1.913(2)		
Od	O15	1.902(2)	1.938(2)	1.928(2)		
Od	O18	1.905(2)	1.934(2)	1.917(2)		

Table S5: Bond length in [Å] and angles in [°] of Ni-N and Ni-O of the transition metal complexes in **II**.

Ni(1)-O(16)	2.158(2)	Ni(2)-N(31)	2.079(3)
Ni(1)-N(2)	2.085(3)	Ni(2)-N(32)	2.082(3)
Ni(1)-N(2)#2	2.085(3)	Ni(2)-N(12)	2.094(3)
Ni(1)-N(1)	2.095(3)	Ni(2)-N(52)	2.111(3)
Ni(1)-N(1)#2	2.095(3)	Ni(2)-N(51)	2.114(3)
Ni(1)-O(16)#2	2.158(2)	Ni(2)-N(11)	2.123(3)
N(2)-Ni(1)-N(2)#2	180.0	N(31)-Ni(2)-N(32)	80.20(13)
N(2)-Ni(1)-N(1)	83.10(13)	N(31)-Ni(2)-N(12)	91.29(12)
N(2)#2-Ni(1)-N(1)	96.90(13)	N(32)-Ni(2)-N(12)	166.96(13)
N(2)-Ni(1)-N(1)#2	96.90(13)	N(31)-Ni(2)-N(52)	168.59(12)
N(2)#2-Ni(1)-N(1)#2	83.10(13)	N(32)-Ni(2)-N(52)	100.04(13)
N(1)-Ni(1)-N(1)#2	180.0	N(12)-Ni(2)-N(52)	90.27(13)
N(2)-Ni(1)-O(16)#2	93.79(10)	N(31)-Ni(2)-N(51)	90.04(12)
N(2)#2-Ni(1)-O(16)#2	86.21(10)	N(31)-Ni(2)-N(51)	90.04(12)
N(1)-Ni(1)-O(16)#2	90.48(10)	N(32)-Ni(2)-N(51)	93.45(13)
N(1)#2-Ni(1)-O(16)#2	89.52(10)	N(12)-Ni(2)-N(51)	96.43(12)
N(2)-Ni(1)-O(16)	86.21(10)	N(52)-Ni(2)-N(51)	78.55(12)
N(2)#2-Ni(1)-O(16)	93.79(10)	N(31)-Ni(2)-N(11)	92.81(12)
N(1)-Ni(1)-O(16)	89.52(10)	N(32)-Ni(2)-N(11)	91.48(13)
N(1)#2-Ni(1)-O(16)	90.48(10)	N(12)-Ni(2)-N(11)	79.01(12)
O(16)#2-Ni(1)-O(16)	180.0	N(52)-Ni(2)-N(11)	98.58(13)
		N(51)-Ni(2)-N(11)	174.66(13)

Table S6. Geometric parameters of hydrogen bonding interactions of H_2O molecules in the structure of **II**.

	Distance [Å]	Angle [°]
O31-H···O32	2.7847(2)	169.223(7)
O31-H···O33	2.7342(1)	158.191(8)
O31-H···O39	2.8656(1)	169.778(8)
O32-H···O34	2.6749(1)	163.207(8)
O33-H···O35	2.7993(1)	149.750(7)
O34-H···O35	2.7532(2)	148.215(6)
O34-H···O36	2.7651(1)	148.297(7)
O35-H···O38	2.8805(2)	158.971(7)
O36-H···O37	2.7458(1)	165.309(7)
O37-H···O38	2.9150(1)	174.463(6)
Interaction with the $[Ni(phen)_3]^{2+}$ complex		
C51-H···O36	2.5726(2)	
C12-H···O37	2.6255(2)	
C56-H···O39	2.5609(1)	
Interaction with the $\{V_{15}Sb_6O_{42}\}$ cluster core		
O31-H···O20	1.9376(1)	
O33-H···O17	2.0236(1)	
O35-H···O19	1.9346(1)	
Interaction with the bridging $[Ni(en)_2]^{2+}$ complex		
O34-H···O16	1.9304(1)	
O34···H-N2	2.60(1)	

Table S7. Geometric parameters of further hydrogen bonding interactions in the structure of **II** with H···A < r(A) + 2.000 Å and DHA > 110°.

D-H	d(D-H)	d(H..A)	d(D..A)	<DHA
N(1)-H(1N1)...O(40)#2	0.91	2.57	3.241(7)	130.7
N(1)-H(2N1)...O(15)	0.91	2.26	3.111(4)	155.8
C(1)-H(1B)...O(22)#2	0.99	2.56	3.536(4)	170.1
N(2)-H(1N2)...O(34)#3	0.91	2.60	3.379(5)	143.6
N(2)-H(2N2)...O(14)#2	0.91	2.28	3.151(4)	160.2
C(12)-H(12)...O(37)#4	0.95	2.63	3.322(6)	130.4
C(19)-H(19)...O(10)	0.95	2.66	3.446(5)	140.7
C(19)-H(19)...O(20)	0.95	2.57	3.438(5)	151.7
C(31)-H(31)...N(12)	0.95	2.63	3.163(5)	115.7
C(32)-H(32)...O(17)#3	0.95	2.47	3.228(5)	136.5
C(39)-H(39)...O(19)#5	0.95	2.53	3.412(6)	154.3
C(51)-H(51)...N(31)	0.95	2.60	3.129(5)	115.8
C(51)-H(51)...O(36)#3	0.95	2.57	3.234(7)	127.1
C(52)-H(52)...O(22)	0.95	2.42	3.072(5)	126.0
C(59)-H(59)...O(8)#6	0.95	2.66	3.549(5)	156.8
C(59)-H(59)...O(22)#7	0.95	2.34	3.023(6)	128.3
O(31)-H(1O)...O(33)	0.84	1.95	2.746(6)	158.7
O(31)-H(2O)...O(20)	0.84	1.94	2.756(4)	164.2
O(32)-H(3O)...O(31)#8	0.84	1.95	2.784(5)	169.2
O(32)-H(4O)...O(34)	0.84	1.86	2.673(6)	163.2
O(33)-H(5O)...O(17)	0.84	1.94	2.728(4)	156.4
O(33)-H(6O)...O(32)	0.84	2.01	2.792(6)	154.9
O(34)-H(7O)...O(35)#8	0.84	2.00	2.751(5)	148.3
O(34)-H(8O)...O(16)#3	0.84	1.93	2.766(4)	171.2
O(35)-H(9O)...O(19)	0.84	2.02	2.777(4)	149.0
O(35)-H(10O)...O(33)	0.84	2.03	2.783(6)	149.5
O(36)-H(11O)...O(34)	0.84	2.00	2.767(6)	152.0
O(36)-H(12O)...O(11)#3	0.84	2.03	2.857(5)	170.0
O(37)-H(13O)...O(38)	0.84	2.08	2.917(6)	174.5
O(37)-H(14O)...O(36)	0.84	1.92	2.746(7)	165.4
O(38)-H(15O)...O(35)#8	0.84	2.08	2.880(5)	158.9
O(39)-H(16O)...O(31)#8	0.86	2.01	2.865(5)	169.8

A labelled cluster anion and a labelled $[Ni(phen)3]^{2+}$ is display in Figure S5. Figure S6 shows the arrangement of the water cluster in the structure.

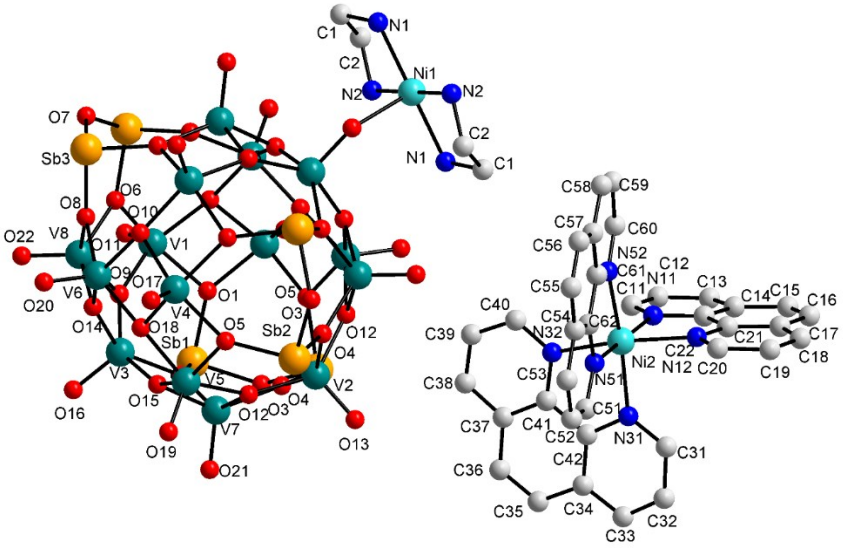

Figure S6: Asymmetric unit of **II** with labeled atoms. Hydrogen atoms are not shown.

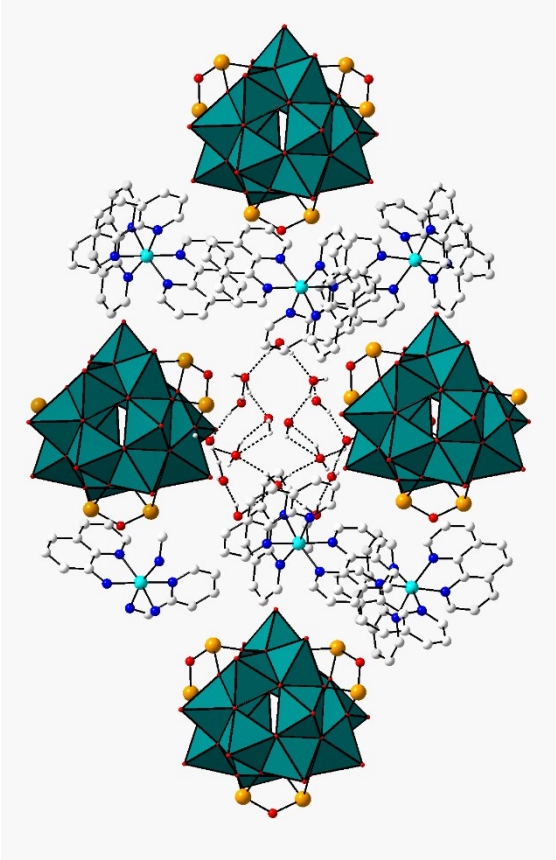

Figure S7: Water cluster occupying the free space between the POV clusters and the $[Ni(phen)_3]^{2+}$ complexes.

Additional magnetochemical analysis

As indicated in the main text, we further elaborate the analysis of the magnetic data. Assuming that the exchange interactions mediated by the Ni^{2+} center within the $\{V_{15}Sb_6\}$–Ni chain is small, the contribution of the Ni^{2+} centers can be estimated by subtracting the $\chi_m T$ vaues[10] of the isolated $[V_{15}Sb_6O_{42}]^{6-}$ anion from the data of **II** until the $\chi_m T$ *vs*. T curve is nearly temperature independent (horizontal) for higher temperatures, as would be expected for (only weakly interacting) Ni^{2+} centers. This requires scaling the $\{V_{15}Sb_6\}$ $\chi_m T$ data by a factor of 0.7–0.8. The scaling may reflect differences in the amount of crystal solvents and the cationic lattice. Due to the shoulder in the $\chi_m T$ data of the $\{V_{15}Sb_6\}$ anion at approximately 160 K, this results, however, in $\chi_m T$ vs. T curves where either the data for T > 160 K is almost constant and continuously decreases for cooling below this temperature (scenario a), factor 0.7), or a maximum is generated at $T \approx 160$ K (scenario b), factor 0.8, see Figure S7). Both scenarios are, however, more or less non-physical: For scenario a), the $\chi_m T$ values at room temperature are distinctly larger than the upper limit of 4.60 cm^3 K mol^{-1} for three non-interacting Ni^{2+} centers, indicating strong ferromagnetic exchange interactions for which, however, there is no evidence at low temperatures. In addition, the decreasing $\chi_m T$ values for T below 160 K cannot be reproduced assuming small $\{V_{15}Sb_6\}$-Ni exchange interactions. Scenario b) can be better reproduced in terms of numerical fitting. Note, however, that the occurrence of the maximum at ca. 160 K is implausible for the observed coordination geometries of the Ni^{2+} centers in **II**. Additionally, the $\chi_m T$ value of 4.53 cm^3 K mol^{-1} is unusually close to the upper limit considering the type of ligands. The least-squares fit employing the "full" model Hamiltonian using the computational framework CONDON 2.0[11,12] assuming in first approximation similar Ni^{2+} centers in a ligand field of D_{4h} symmetry and considering the exchange interactions in a mean-field approach yields a fit of quality SQ = 1.0% which is deceptively good. The Ni^{2+} ligand field parameters (Wybourne notation) B^2_0 = –31200 cm^{-1}, B^4_0 = 15050 cm^{-1} and B^4_4 = 8000 cm^{-1} represent, however, a tetragonal and strongly distorted ligand field, in contrast to the X-ray diffraction structural data, and the maximum at 160 K cannot be reproduced. The magnetization curve is reasonably

reproduced with a value of 6.6 N_A μ_B at 5.0 T. The exchange interactions determined by the mean–field approach for the Ni^{2+} center in the chain is zJ = –0.4 cm^{-1} ("–2J" notation for Heisenberg exchange interaction, and z = 2 for a chain) indicating weak antiferromagnetic exchange interaction. All in all, while the assumption of weak exchange interactions seems to be roughly justified, the other results are somewhat off the expectation. The bridging Ni^{2+} centers also seem to slightly modify the exchange interactions within the polyoxovanadate anions of the chain in **II** compared to the isolated anion since the data show the approximately linear $\chi_m T$ behavior starting at much lower temperatures (T > 25 K) than for the isolated anion (T > 160 K).

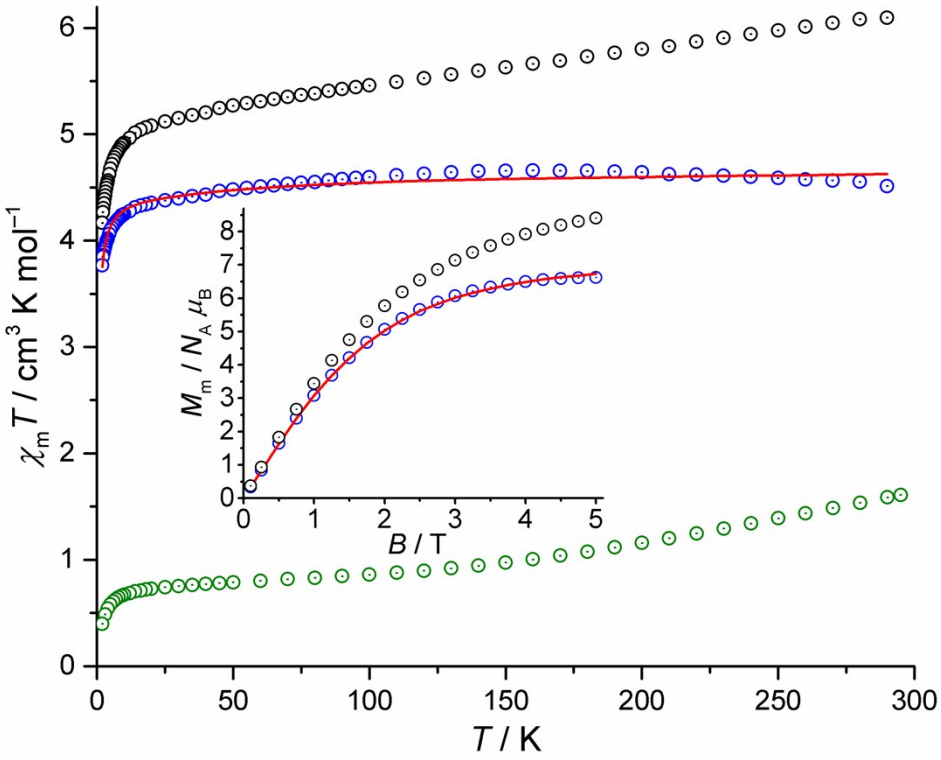

Figure S8. Magnetic data of **II**: $\chi_m T$ *vs*. temperature T at 0.1 T; inset: molar magnetization M_m *vs*. magnetic field B at 2.0 K. Black circles: experimental data; green circles: $\chi_m T$($[V_{15}Sb_6O_{42}]^{6-}$) (scaled);[10] blue circles: differences of data of compound **II** and the $\{V_{15}Sb_6\}$ anion; red lines: least–squares fits.

[1] M. Wendt, U. Warzok, C. Näther, J. van Leusen, P. Kögerler, C. A. Schalley, W. Bensch, *Chem. Sci.* **2016**, *7*, 2684.
[2] M. O'Keeffe, N. E. Brese, *J. Am. Chem. Soc*. **1991**, *113*, 3226.
[3] E. Antonova, C. Näther, P. Kögerler, W. Bensch, *Angew. Chem*. **2011**, *123*, 790 .

[4] R. Kiebach, C. Näther, P. Kögerler, W. Bensch, *Dalton Trans*. **2007**, 3221.
[5] E. Antonova, C. Näther, W. Bensch, *Dalton Trans*. **2012**, *41*, 1338.

[6] E. Antonova, C. Näther, W. Bensch, *CrystEngComm* **2012**, *14*, 6853.

[7] A. Wutkowski C. Näther, P. Kögerler, W. Bensch, *Inorg. Chem*. **2013**, *52*, 3280.

[8] E. Antonova, C. Näther, P. Kögerler, W. Bensch, *Inorg. Chem*. **2012**, *51*, 2311.

[9] E. Antonova, B. Seidlhofer, J. Wang, M. Hinz, W. Bensch, *Chem. Eur. J.* **2012**, *18*, 15316.

[10] R. Kiebach, C. Näther, P. Kögerler, W. Bensch, *Dalton Trans.*, **2007**, 3221.

[11] M. Speldrich, H. Schilder, H. Lueken, P. Kögerler, *Isr. J. Chem.* **2011**, 51, 215.

[12] J. van Leusen, M. Speldrich, H. Schilder, P. Kögerler, *Coord. Chem. Rev.* **2015**, *289*, 137.